Journal of *Marine Science and Engineering*

MDPI

Article

Model Construction of Wave Energy Array Limiting System and Analysis of Power Generation Capacity in Real Sea Conditions

Mingze Ji [1], Sizhang Rong [1], Meiyu Jiang [1], Jialong Li [1,*], Wenbin Lai [2] and Xiongbo Zheng [1]

[1] School of Mathematics Science, Harbin Engineering University, Harbin 150001, China; jimingze0926@126.com (M.J.); sizhangrong@gmail.com (S.R.); jmy15045232127@163.com (M.J.); zhengxiongbo@hrbeu.edu.cn (X.Z.)
[2] School of Mechanical Engineering and Intelligent Manufacturing, NingBoTech University, Ningbo 315100, China; laiwenbin@nbt.edu.cn
* Correspondence: ljlhhh@hrbeu.edu.cn

Abstract

Wave energy converter (WEC) arrayization is a crucial direction for the large-scale utilization of wave energy. However, under real sea states, irregular waves, displacement overruns under severe motion conditions, and insufficient adaptability of fixed damping control pose difficulties for power generation capacity assessment. In this paper, a motion-limiting system model is established to address the severe motion of floating bodies under extreme conditions. A state-space model is employed to replace the numerical integration method for calculating the convolution term in the time-domain motion equation. Combined with the distribution of real sea state data, a variable parameter control method based on latch control is proposed using the optimal limiting damping parameters. The power generation matrices and energy capture widths under different sea states in an actual sea area in 2022 are calculated, and the annual power generation under regular and irregular wave assumptions is computed. The results show that, compared with linear control, the average power of Floating Body 1 under variable parameter control increases from 18.116 kW to 20.092 kW, and that of Floating Body 2 increases from 35.146 kW to 45.140 kW. These results provide a quantitative basis for the engineering design and control strategy selection of WEC arrays in actual sea areas.

Keywords: wave energy converter array; motion-limiting system; power generation assessment

Check for updates

Academic Editor: Eugen Rusu

Received: 30 September 2026
Revised: 10 October 2026
Accepted: 13 October 2026
Published: 14 October 2026

Copyright: © 2026 by the authors. Licensee MDPI, Basel, Switzerland. This article is an open access article distributed under the terms and conditions of the Creative Commons Attribution (CC BY) license.

1. Introduction

Among the various forms of ocean energy, wave energy has attracted widespread attention due to its wide distribution, high energy flux density, and theoretical global reserves of 3.65 TW [1]. Compared with renewable energy sources such as wind and solar energy, its relatively stable energy supply mode makes wave energy more available. Promoting the large-scale development and utilization of wave energy is an important way to alleviate the contradiction between energy supply and demand, and is also a key direction for achieving energy structure transformation and low-carbon development.

According to the working principles of WEC systems, they can be classified into oscillating water column (OWC) type, overtopping type, and oscillating body type. Among them, the point absorber WECs within the oscillating body type can be further divided

into single-body, two-body, and array configurations [2–5]. The point absorber WECs within the oscillating body type exhibit strong environmental adaptability and high energy conversion efficiency, making them more suitable for modular design and large-scale array deployment. The energy capture mechanism of oscillating body WECs relies on the multi-degree-of-freedom response of the floating body under wave excitation to drive the PTO system, thereby converting wave energy into mechanical energy and then into electrical energy. To improve the energy capture efficiency of the device by controlling the PTO system, it is crucial to accurately obtain the hydrodynamic parameters of the floating body under wave loads. Hydrodynamic characteristic research methods can be categorized into analytical solutions based on potential flow theory, boundary element methods (BEM), and CFD methods based on viscous flow theory [6–8]. In 2023, Das [9] developed an analytical hydrodynamic model for a horizontal elliptical disk in a two-layer fluid based on elliptic coordinates. In 2024, Ancellin [10] proposed a computational method using low-rank matrix decomposition to approximate sub-blocks of the matrix, aiming to reduce the computational cost of solving hydrodynamic coefficients using the BEM method. Natarajan [11] applied a viscosity-corrected potential flow theory method to a two-body wave energy device with two concentric cylinders in relative motion, solving for the viscous damping generated by the vortex formation at the edge of the annular outer cylinder during heave motion.

The calculation of the motion of a WEC in waves is fundamental to analyzing its energy conversion characteristics. Numerical calculation methods can be categorized into frequency-domain and time-domain methods. Frequency-domain methods are based on linear assumptions and are suitable for the steady-state response of floating bodies under sinusoidal excitation. By neglecting the time term, the dynamic equations are transformed into the frequency domain to calculate the motion amplitude of the device at different frequencies [12–14]. For problems that frequency-domain methods cannot handle, such as random waves, PTO system nonlinearity, and multi-degree-of-freedom issues, time-domain methods can directly solve the time-history motion of the floating body. Additionally, for linear problems that frequency-domain methods can handle, frequency-domain calculations can also provide solutions, but the computational speed is relatively slow. From an engineering practical perspective, time-domain calculations often adopt the indirect time-domain method, which utilizes the Cummins impulse response to achieve frequency-time domain transformation, and the convolution term in the time-domain motion equation can be directly discretized and solved. The direct numerical integration method for the convolution term becomes a computational burden because it requires solving with different data at each time step. Some scholars have improved this by using radiation force approximation methods. In 1984, Jefferys [15] employed a state-space model to approximate the convolution term. In 1998, Paul [16] proposed the Prony method, which uses a complex exponential sum to approximate the impulse response function to handle the convolution term. Regarding the above three commonly used methods for calculating the convolution term, in 2015, Armesto [17] summarized and compared these three methods. Compared with the direct solution of the convolution term, the state-space approximation and Prony coefficient approximation methods effectively save computational cost.

Previous studies on WEC devices that were shut down or damaged during sea trials have revealed that the end-stop collision problem of the PTO system is one of the main issues hindering the survivability of wave energy converters under severe motion conditions [18]. In 2017, Sjökvist [19] installed limit springs at both ends of a point absorber wave energy device to address the end-stop collision problem of the PTO system in extreme waves and tsunamis. In 2019, Wei [20] evaluated the power absorption capacity of

the Ocean Grazer wave energy device, which consists of a point absorber array, under different nonlinear PTO configurations. In 2022, Shahroozi [21] investigated the nonlinear phenomena and the influence of PTO damping on the motion response of a point absorber wave energy device equipped with a motion-limiting mechanism under severe motion conditions and intermediate water depths. In 2024, Zheng Xiongbo [22] proposed a parameter optimization design method for a built-in two-body wave energy device with a motion-limiting system. Therefore, to improve the energy capture efficiency of wave energy devices, it is necessary to conduct in-depth research on the motion response and energy conversion characteristics of floating bodies under a PTO system equipped with a motion-limiting mechanism. To address the above issues, this paper takes a two-floater WEC array as the research object, establishes a time-domain motion model incorporating a motion-limiting system, employs a state-space model to accelerate the calculation of the convolution term, proposes a variable parameter control method based on latch control, and evaluates the annual power generation in the sea area of 111~113° E, 15.5~17° N based on ERA-5 reanalysis data.

2. Array Model and Numerical Simulation of Irregular Waves

In this paper, a wave energy converter (WEC) array composed of two cylindrical floating bodies is taken as the research object, and a two-floater array model is established as shown in Figure 1. Considering the differences in hydrodynamic forces and energy capture characteristics of floating bodies at different positions in actual engineering, the two selected floating bodies exhibit significant differences in geometric dimensions. The floating body with a smaller radius and draft is defined as Floating Body 1, and the floating body with a larger radius and draft is defined as Floating Body 2. Among them, Floating Body 1 has a radius ratio of R_1/h = 0.2 and a draft ratio of d_1/h = 0.2, while Floating Body 2 has a radius ratio of R_2/h = 0.3 and a draft ratio of d_2/h = 0.35. The center-to-center distance is L_{12} = 0.7 h.

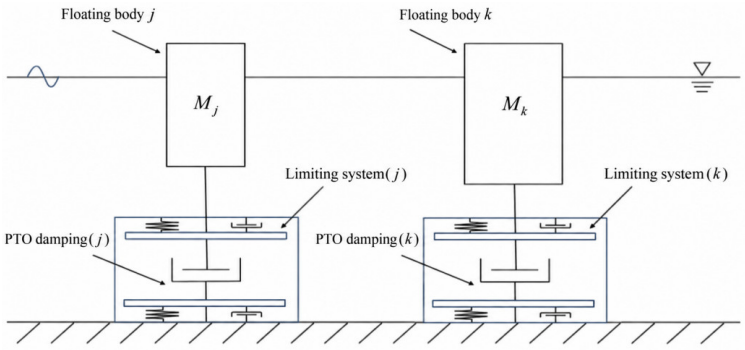


Figure 1. Motion-limiting model of the WEC array.

The parameters of the WEC floater are listed in Table 1. The added mass, radiation damping, wave excitation force amplitude, and excitation force phase were calculated using the hydrodynamic software ANSYS 2022. The simulation of the irregular wave excitation force can be expressed as

$$F_e = \int_{-\infty}^{\infty} K_e(\tau)\eta(t-\tau)d\tau \quad (1)$$

where K_e is the impulse response function of the excitation force. In the numerical simulation, the above integral needs to be truncated for computation, and the generation of the irregular wave surface time-history curve is the focus of the calculation.

Table 1. Parameters of the WEC floating body.

Parameter	Body 1	Body 2
Mass (kg)	25,740	101,390
Radius (m)	2	3
Draft (m)	2	3.5
Restoring coefficient (N/m)	126,200	284,090
limiting damping (N·m/s)	4×10^8	4×10^8
limiting spring (N·m)	151,440	340,908
Water depth (m)	10	

To provide a benchmark for the subsequent energy conversion optimization of the array, we first analyze the optimal performance of a single device under ideal conditions. Assume that the optimal output power of an isolated wave energy converter is $P_{isolated}(\omega)$. At this time, the PTO damping is the optimal PTO damping, which is obtained by $\partial P_{isolated}(\omega)/\partial c_{p,iso} = 0$, where $c_{p,iso}$ is

$$c_{p,iso} = \sqrt{[K/\omega - \omega(M+\mu)]^2 + \lambda^2} \tag{2}$$

Considering the optimal output power of two wave energy converters, such that $\partial P_1(\omega)/\partial c_{p,1} = 0$ and $\partial P_2(\omega)/\partial c_{p,2} = 0$ are satisfied respectively, can obtain

$$\begin{cases} c_{p,1_opt} = \frac{1}{\omega}\sqrt{\frac{(S_3+c_{p,2}{S_4}^{(1)})^2+(S_5+c_{p,2}{S_6}^{(1)})^2}{{S_1}^{(1)2}+({S_2}^{(1)}+\omega c_{p,2})^2}} \\ c_{p,2_opt} = \frac{1}{\omega}\sqrt{\frac{(S_3+c_{p,1}{S_4}^{(2)})^2+(S_5+c_{p,1}{S_6}^{(2)})^2}{{S_1}^{(2)2}+({S_2}^{(2)}+\omega c_{p,1})^2}} \end{cases} \tag{3}$$

where P_1 and P_2 are the average power of WEC 1 and WEC 2, respectively:

$${S_1}^{(1)} = \omega^2(M_2+\mu_{22}) - K_2, {S_1}^{(2)} = \omega^2(M_1+\mu_{11}) - K_1, {S_2}^{(1)} = \omega\lambda_{22}, {S_2}^{(2)} = \omega\lambda_{11},$$
$$S_3 = \omega^4[(M_1+\mu_{11})(M_2+\mu_{22}) - \mu_{12}^2] + K_1K_2 + \omega^2[-(M_1+\mu_{11})K_2 - (M_2+\mu_{22})K_1 - \lambda_{11}\lambda_{22} + \lambda_{12}^2],$$
$${S_4}^{(1)} = -\omega^2\lambda_{11}, {S_4}^{(2)} = -\omega^2\lambda_{22}, S_5 = \omega^3[\lambda_{22}(M_1+\mu_{11}) + \lambda_{11}(M_2+\mu_{22}) - 2\mu_{12}\lambda_{12}] - \omega[\lambda_{11}K_2 + \lambda_{22}K_1]$$
$${S_6}^{(1)} = \omega^3(M_1+\mu_{11}) - \omega K_1, {S_6}^{(2)} = \omega^3(M_2+\mu_{22}) - \omega K_2$$

The above optimal PTO damping is derived based on regular waves. However, the waves in the actual ocean environment are random and irregular. To further analyze the hydrodynamic characteristics of the WEC array under real sea states, it is necessary to first accurately simulate the wave environment under actual sea conditions. Therefore, this paper employs the linear wave superposition method [23] to carry out the numerical simulation of irregular waves. Based on a stationary random process, the ocean waves are regarded as the linear superposition of an infinite number of cosine waves with different periods and random initial phases. Let the number of component waves be M; then, the wave surface equation can be written as

$$\eta(t) = \sum_{i=1}^{M} a_i \cos(k_i z - \omega_i t + \varepsilon_i) \tag{4}$$

where a_i, k_i and ω_i are the amplitude, wave number, and circular frequency of the i-th component wave, respectively; z and t represent position and time; ε_i is the initial phase of the i-th component wave, which is a random number uniformly distributed within (0,2π). The wave number and original frequency can be expressed by the wavelength L and period T:

$$k_i = 2\pi/L_i, \quad \omega_i = 2\pi/T_i \tag{5}$$

To determine the amplitude a_i of each component wave, a wave spectrum needs to be introduced. Therefore, this paper adopts the improved JONSWAP spectrum as the target spectrum, and its expression is

$$S(\omega) = \beta_j 5\pi^4 \frac{{h_{1/3}}^2}{T_P^4} \frac{1}{\omega^5} \exp[-\frac{20\pi^4}{T_P^4} \cdot \frac{1}{\omega^4}] \gamma^{\exp[-(\omega-\omega_p)^2/(2\sigma^2\omega_p^2)]} \tag{6}$$

where ω_p is the peak frequency, the peak period $T_P^4 = 2\pi/\omega_p$ is the significant wave height, γ is the peak enhancement factor, and σ is the shape parameter of the spectrum:

$$\sigma = \begin{cases} 0.07(\omega \le \omega_p) \\ 0.09(\omega > \omega_p) \end{cases} \tag{7}$$

In the numerical simulation, the continuous spectrum needs to be discretized. Let the spectral frequency range (ω_L,ω_H) cover the vast majority of the energy, and divide it equally into M parts with an interval of $\Delta\omega_i = \omega_i - \omega_{i-1}$. Taking the following,

$$\begin{aligned} \hat{\omega}_i &= (\omega_{i-1} + \omega_i)/2 \\ a_i &= \sqrt{2S_m(\hat{\omega}_i)\Delta\omega_i} \end{aligned} \tag{8}$$

Then, the irregular wave surface equation obtained by superposing M cosine waves can be expressed as

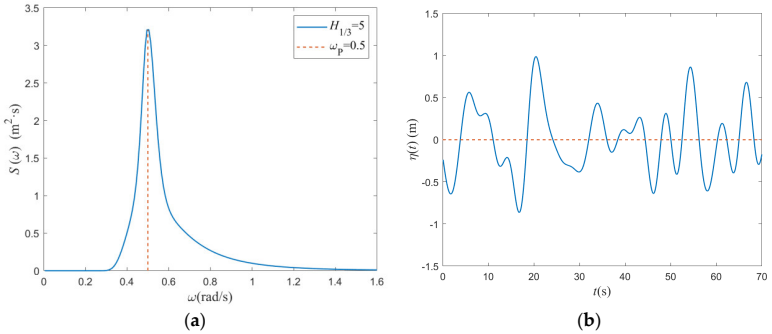
$$\eta(t) = \sum_{i=1}^{M} \sqrt{2S_m(\hat{\omega}_i)\Delta\omega_i} \cos\left(\widetilde{\omega}_i t + \varepsilon_i\right) \tag{9}$$

Therefore, the incident wave power per unit width of irregular waves is expressed as

$$P_W = \sum_{i=1}^{M} \frac{1}{2}\rho g a_i^2 \frac{\widetilde{\omega}_i}{\widetilde{2k}_i} \left[1 + \frac{\widetilde{2k}_i h}{\sinh\left(\widetilde{2k}_i h\right)}\right] = \sum_{i=1}^{M} \rho g S_m(\hat{\omega}_i)\Delta\omega_i \frac{\widetilde{\omega}_i}{\widetilde{2k}_i} \left[1 + \frac{\widetilde{2k}_i h}{\sinh\left(\widetilde{2k}_i h\right)}\right] \tag{10}$$

where $\widetilde{k}_i$ is the representative wave number of the i-th wave.

Based on the above formulas, the JONSWAP spectrum with a specified significant wave height and peak frequency is selected for the numerical simulation of irregular waves. Figure 2 presents the simulation results of the irregular waves, where Figure 2a shows the adopted JONSWAP spectral shape, and Figure 2b shows the wave surface time-history curve generated by superposition according to the formulas. It can be seen from the figure that the generated wave surface exhibits obvious randomness and irregularity in the time domain, which is consistent with the characteristics of actual ocean waves.



(**a**) (**b**)

Figure 2. Numerical simulation of irregular waves. (**a**) Description of JONSWAP spectrum. (**b**) Description of the time-history curve of the wave surface.

3. Motion-Limiting System of the WEC Array and Solution of the Time-Domain Motion Equation

The marine environment is complex and changeable. Under severe motion conditions, the heave motion of the floating body intensifies. If the floating body resonates with the waves at this time, it will suppress the energy absorption capacity of the device and even cause safety problems. To meet the dynamic stability requirements of the floating body in the marine environment, a motion-limiting design method is proposed as shown in Figure 1, which preserves the motion response in the main energy capture frequency band while suppressing the extreme displacement risk of the WEC, thereby improving the energy capture efficiency of the device and its survivability under severe motion conditions.

3.1. State-Space Model

To avoid severe motion of the floating body, a motion-limiting system is installed to prevent the floating body from exceeding the design threshold, thereby controlling the heave motion of the floating body within a certain range. The PTO force can be expressed as:

$$f_{pto,j}(t) = \begin{cases} c_{p,j}\dot{z}_j(t) & |z_j(t)| \le L_j \\ (c_{p,j} + c_{L,j})\dot{z}_j(t) + k_{L,j}z_j(t) & |z_j(t)| > L_j \end{cases} \tag{11}$$

where $c_{L,j}$ is the motion-limiting damping coefficient of the j-th device in the WEC array, and L_j is the designed maximum displacement of the j-th floating body. In our previous studies [24], setting a larger limit damping coefficient yielded better power generation performance; therefore, in the limit model of this paper, $c_{L,j} = 4 \times 10^8$ N/(m/s) and $k_{L,j} = 1.2\ K_j$.

Due to the introduction of the motion-limiting system, the PTO force exhibits piecewise nonlinear characteristics, and traditional frequency-domain methods are no longer applicable. Therefore, a time-domain motion equation must be established for the solution. According to Cummins' theory, during the calculation process, it is necessary to handle the convolution term that characterizes the free-surface memory effect. However, directly solving this convolution term using numerical integration methods results in low time-domain computational efficiency. Therefore, this paper adopts a state-space model to replace the convolution term to effectively solve this problem. The state-space model is as follows:

$$\begin{cases} \dot{y}(t) = A'y(t) + B'\dot{z}_j(t) \\ \int_0^t k(t-\tau)\dot{z}_j(\tau)d\tau \approx C'y(t) + D'\dot{z}_j(t) \end{cases} \tag{12}$$

where $c_{L,j}$ is the motion-limiting damping coefficient of the j-th device in the WEC array, and L_j is the designed maximum displacement of the j-th floating body.

Where $y(t)$ is the state vector matrix with a dimension of $n \times 1$; the dimensions of the constant coefficient matrices $y(t)$, B', C' and D' are $n \times n$, $n \times 1$, $1 \times n$ and 1×1, respectively; the velocity $\dot{z}_j(t)$ of cylinder j and the convolution term $\int_0^t k(t-\tau)\dot{z}_j(\tau)d\tau$ are the input and output of this state space, respectively.

The key to establishing the above state-space model lies in accurately obtaining the four constant coefficient matrices, whose accuracy directly determines the accuracy of the convolution term replacement. First, the delay function $k(t)$ is solved for system identification, and the realization theory method is selected for parameter estimation [25]. Under the condition of ensuring model stability, the lowest order n of the system is found. The transformation relationship between $k(t)$ and the state space is utilized to obtain $y(t)$, B', C' and D'. Meanwhile, in actual calculations, neglecting the discretization term D' of the continuous system often yields a better approximation.

In the two-floater array studied in this paper, due to the hydrodynamic coupling between the two floating bodies, the delay function $k(t)$ is extended to a 2×2 matrix. The delay functions obtained by the numerical integration method and the indirect solution via realization theory are compared, and the results of each term in the experimental function matrix $k(t)$ are shown in Figure 3. The delay function curves obtained by different methods agree well, indicating that the method of using the state-space model to replace the convolution term for time-domain numerical simulation is feasible.

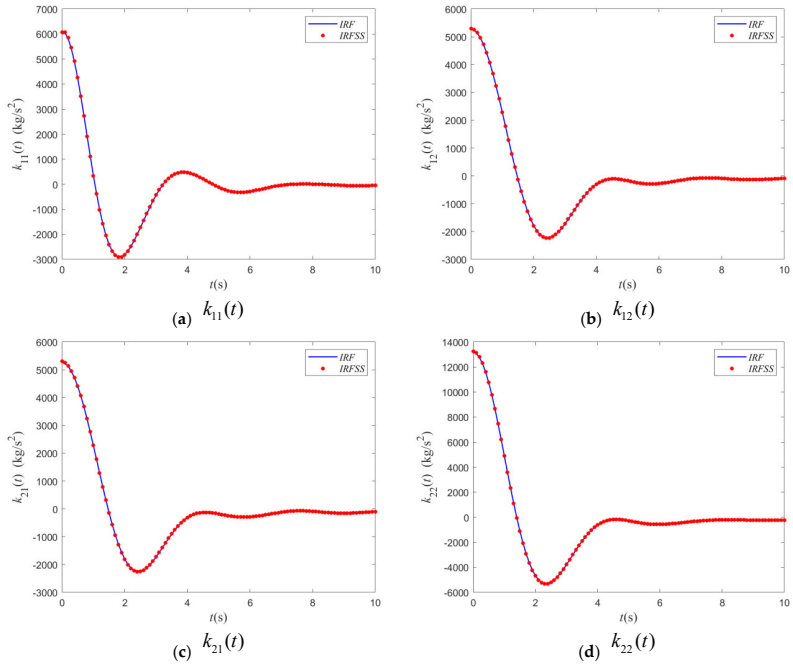


Figure 3. Delay Function.

3.2. Time-Domain Motion Equation of the Motion-Limiting System and Numerical Solution

Based on the above formulas, the time-domain motion equation is obtained by replacing the convolution term with the state-space model.

$$\begin{cases} [M_1 + \mu_{11}(\infty)]\ddot{z}_1(t) + C'_{11}y_{11} + D'_{11}\dot{z}_1(t) + C'_{12}y_{12} + D'_{12}\dot{z}_2(t) + K_1 z_1(t) \\ \quad +\mu_{12}(\infty)\ddot{z}_2(t) - c_{pL,1}(t)\dot{z}_1(t) - k_{pL,1}(t)z_1(t) = F_{e,1}(t) \\ [M_2 + \mu_{22}(\infty)]\ddot{z}_2(t) + C'_{21}y_{21} + D'_{21}\dot{z}_1(t) + C'_{22}y_{22} + D'_{22}\dot{z}_2(t) + K_2 z_1(t) \\ \quad +\mu_{21}(\infty)\ddot{z}_1(t) - c_{pL,2}(t)\dot{z}_2(t) - k_{pL,2}(t)z_2(t) = F_{e,2}(t) \\ \dot{y}(t) = A'y(t) + B'\dot{z}(t) \end{cases} \tag{13}$$

The motion equation of the two-floater array can be written in matrix form as

$$\dot{X} = PX + Q \tag{14}$$

Based on the nonlinear time-domain coupled motion equations established above, this paper will verify the effect of the motion-limiting system through time-domain numerical simulation. To comprehensively evaluate the adaptability of the model under different sea states, the time-history curves of the floating body motion under two conditions—with and without motion limiting—are calculated and compared under regular and irregular wave excitations, respectively, at an incident wave direction angle of 0 and ω = 1.5182.

Under regular wave excitation, the time-history motions of both floating bodies exhibit significant periodic characteristics, as shown in Figure 4. When the motion-limiting system is not considered, the heave reciprocating motion amplitude of the two floating bodies is larger, and the trend is stable. Considering the effective physical stroke limitation of

the device in actual engineering, and to avoid mechanical collision of the system, the motion-limiting system displacement thresholds for the two floating bodies in the WEC array are set to L_1 = 1.2 m and L_2 = 0.8 m, respectively. It can be found from the figure that the heave displacements of each floating body are within the design thresholds. Due to the regulation of the damping motion-limiting system and the hydrodynamic coupling between the WEC array, the heave motions of the floating bodies influence each other.

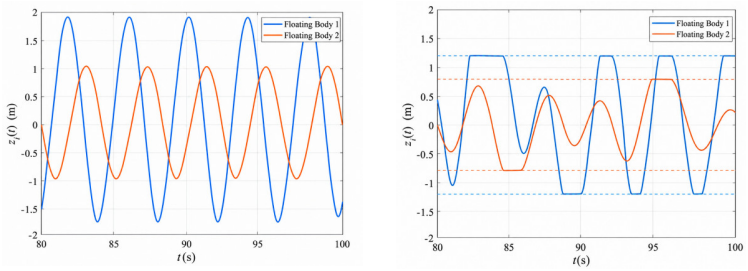


Figure 4. Time-history curves of the two-floater array motion with and without the motion-limiting system (regular waves). (**a**) Floating body motion without a motion-limiting mechanism under regular waves. (**b**) Floating body motion with L_1 = 1.2 m and L_2 = 0.8 m under regular waves.

Under irregular wave excitation, the motion of the floating body exhibits randomness, as shown in Figure 5. When the motion-limiting system is not considered, certain wave surface environments cause the floating body to undergo severe heave motion. To ensure the stability and safety of the entire WEC system, suppressing the instantaneous displacement is necessary at this time. At this point, the advantage of the motion-limiting system in Figure 5b is fully demonstrated. The setting of the displacement thresholds plays a key role, strictly limiting the heave motion of the floating body within the design range and avoiding the risk of severe motion caused by resonance between waves and the floating body under large wave heights and long periods. In the design of the damping motion-limiting system for a WEC array, different thresholds can be set by considering the geometric structures of different floating bodies. This allows some floating bodies to retain a certain dynamic response capability when the overall motion is relatively stable, thereby ensuring the energy capture efficiency of the entire WEC array.

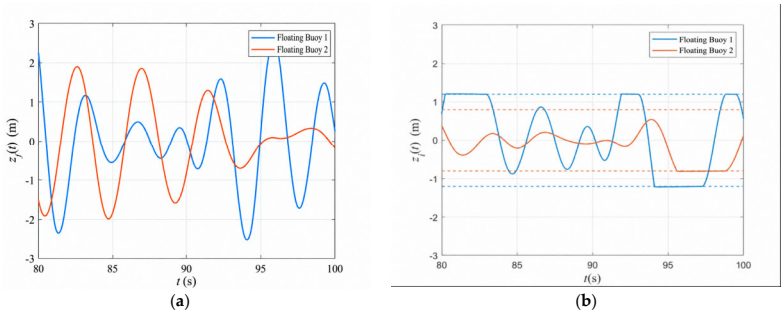


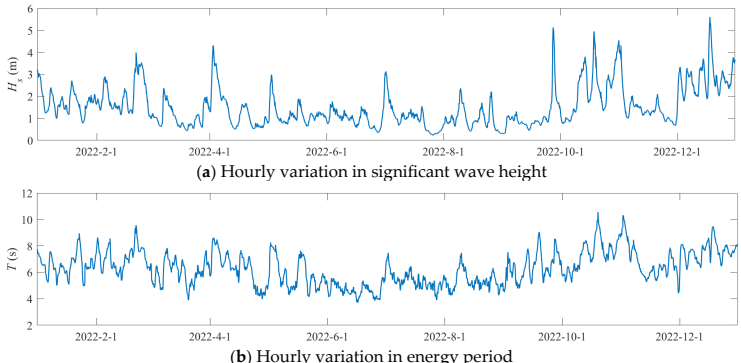
Figure 5. Time-history curves of the two-floater array motion with and without the motion-limiting system (irregular waves). (**a**) Floating body motion without a motion-limiting mechanism under irregular waves. (**b**) Floating body motion with L_1 = 1.2 m and L_2 = 0.8 m under irregular waves.

4. Analysis of Power Generation Capacity of the WEC Array in Real Sea States

The wave resources in the real marine environment exhibit significant seasonal and random variations. Relying solely on numerical simulation makes it difficult to comprehensively evaluate the long-term power generation performance of the device under actual sea states. Therefore, to further investigate the effectiveness of the motion-limiting system in

actual engineering environments, this section conducts a systematic analysis of the power generation capacity of the WEC array based on real ocean wave observation data.

To obtain input data for real sea states, the ERA-5 wave reanalysis data with a spatial resolution of 0.5° × 0.5°, a temporal resolution of 1 h, and a time range covering the entire year of 2022 are selected to statistically analyze the significant wave height and energy period in the sea area of 111~113° E, 15.5~17° N. The statistical results are shown in Figure 6, where the energy period is approximately equal to 0.9 times the peak period. Figure 6c shows the region covered by the ERA5 data, where the data selected in this study correspond to a single grid point within this region. Only the wave data from 2022 were used in this paper, which represents the power generation performance at this grid point for that single year and thus lacks statistical representativeness.



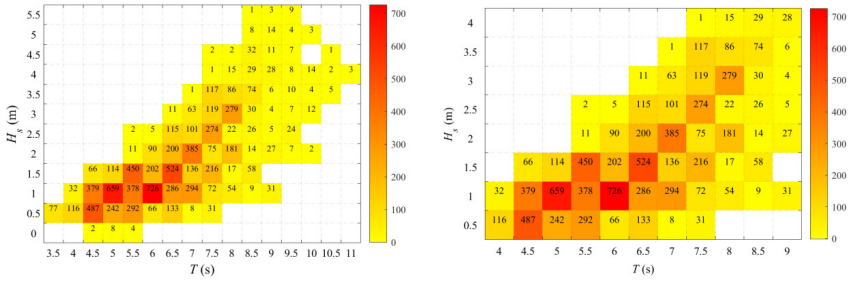
(**a**) Hourly variation in significant wave height

(**b**) Hourly variation in energy period

(**c**) Sea area near the Xisha Islands, China.

Figure 6. Hourly variation in significant wave height and energy period.

The ERA-5 wave reanalysis data yield significant wave height and peak period data ranges of 0.23~5.61 m and 3.70~10.56 s, respectively, where both the wave height and period data are reanalysis data obtained after processing the wave surface time-history, rather than direct observation data. To better illustrate the composition of wave energy resources in terms of wave period and wave height, Figure 7 employs a combined energy and scatter plot approach to statistically analyze the annual sea state data of the sea area. The wave energy is mainly provided by significant wave heights of 0~5.5 m and peak periods of 3.5~11 s. The sub-regions within the combined energy scatter plot are divided into standard grids of 0.5 m and 0.5 s, with 0.25 m and 0.25 s as the interval radii, and the midpoint of each interval is taken as the representative value of wave height and period for that interval. The number of wave height and period data falling into each grid—i.e., the number in each grid cell—represents the occurrence frequency (number of hours) of wave conditions with that peak period and significant wave height. The lower numbers in the upper region of the figure indicate a lower probability of larger waves occurring in the sea area. By observing the number of hours of occurrence for different significant wave heights and peak period sea states, it can be found that for sea states with significant wave heights of 0.5~4 m and peak periods of 4~9 s, the occurrence time accounts for more than 90% of the entire year. The sea state distribution data are shown in Figure 7b. Since the range of the original sea state data is relatively large, the reduced combined energy scatter plot is used to replace the original sea state data, and subsequent calculations are performed on this basis.



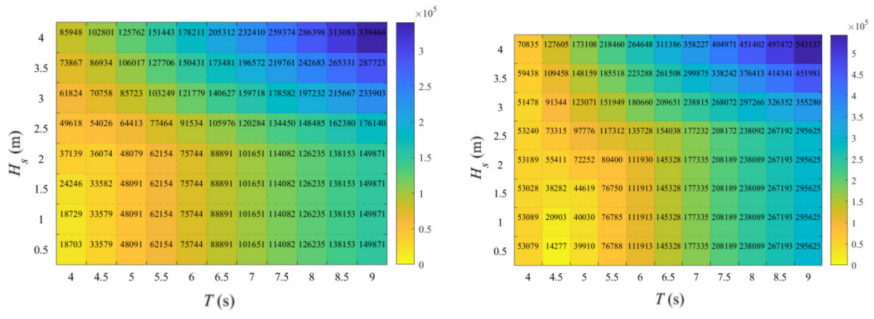
(**a**) Original sea states (**b**) Substituted sea states

Figure 7. Distribution of sea state data in the sea area under different sea states.

4.1. Optimal Motion-Limiting Damping Coefficient of the Device Under Regular Waves

For a WEC array equipped with a damping motion-limiting system, the energy absorbed by the device reaches its maximum when the PTO system is not in contact with the limiting plate. Under irregular waves, since ocean waves are a random process, the wave surface is highly irregular and non-repeatable in both the time and space domains, making it difficult to obtain the optimal parameters of the PTO system. In contrast, under the assumption of regular waves, the damping can be set so that the displacement of the floating body just reaches the design threshold when the motion response is severe, ensuring that the limiting plate does not affect the heave motion of the floating body. To maximize the absorbed power of each device in the WEC array, motion limiting is applied on the basis of Equation (2), where $k_{pL,j} = 0$ and $c_{pL,j} = c_{p,j}$. The optimal PTO damping $c_{p,j_opt} = c_{p,j}$ is defined as the "optimal motion-limiting damping coefficient." The optimal motion-limiting damping coefficient matrix under the sea state data distribution is then easily obtained, where the design thresholds are $L_1 = 1.2$ m and $L_2 = 0.8$ m. The results are as follows.

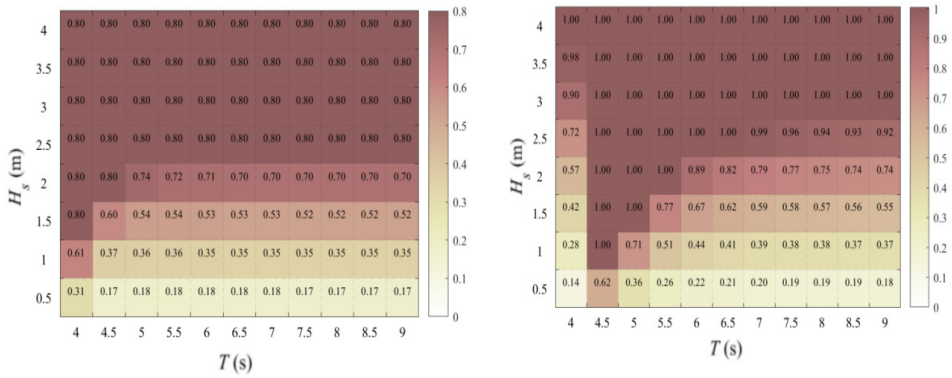
As shown in Figure 8, both floating bodies exhibit a trend where the motion-limiting damping value increases as the energy period becomes longer and the significant wave height becomes larger, where the optimal damping is calculated by Equation (3). Due to its mass being far greater than that of Floating Body 1, Floating Body 2 generally requires higher damping to cope with variations in sea states. At the same frequency, the data repetition in the damping values under low significant wave heights originates from the fact that the PTO damping control using Equation (2) is independent of wave height. The optimal motion-limiting damping values of the WEC array under different sea states increase with the increase in wave height and period, indicating that damping needs to be gradually increased in long-period large waves to suppress the severe motion of the floating bodies.



(**a**) (**b**)

Figure 8. Optimal motion-limiting damping of the two-floater array under different sea states. (**a**) Optimal motion-limiting damping of Floating Body 1 (N·m/s); (**b**) optimal motion-limiting damping of Floating Body 2 (N·m/s).

The displacement limitation of the two floating bodies under optimal motion-limiting damping is shown in Figure 9. Under wave excitation, when the heave motion of the floating body is below the design threshold, there is no need to apply motion-limiting damping control. When the significant wave height is relatively large and the floating body undergoes severe motion, the damping motion-limiting method can be adopted to effectively suppress the motion of the floating body so that it just satisfies the design threshold.



(**a**) RAO of Floating Body 1 (m/m) (**b**) RAO of Floating Body 2 (m/m)

Figure 9. RAO of the two-floater array under optimal motion-limiting damping.

4.2. Variable Parameter Control Method Under Irregular Waves

To achieve optimal energy conversion performance of a point absorber WEC, it is necessary to maintain phase synchronization between the floating body's motion velocity and the wave excitation force. To achieve this condition, a control method is required that locks the floating body's motion when the body velocity vanishes and the wave excitation force and the floating body's motion direction are different, and releases the floating body otherwise. This method is called latch control [26]. Meanwhile, for the damping motion-limiting system of a WEC array, since irregular waves under the same sea state are a random process, it is impossible to make the floating body displacement satisfy the design threshold in real time by using a fixed $c_{p,j}$ value under wave excitation within a certain time period. That is, the time-varying wave parameters cause c_{p,j_opt} to lose its motion-limiting function, and the motion-limiting system will inevitably act to restrict the motion of the floating body. Therefore, a variable parameter control method based on latch control is proposed, which optimizes the motion-limiting constraint by dynamically adjusting the damping coefficient, thereby improving the power absorption capacity of the WEC array. The premise of this method is that the significant wave height, peak period, and wave excitation force of the wave surface under real sea states can be obtained in real time.

When the locking mechanism is triggered, a reverse force is applied by the system to make the velocity and acceleration of the floating body zero. The motion equation of the device at this stage becomes

$$\begin{cases} \ddot{z}_1(t) = 0, \ddot{z}_2(t) = 0 \\ \dot{z}_1(t) = 0, \dot{z}_2(t) = 0 \\ \dot{y}(t) = A'y(t) \end{cases} \tag{15}$$

During the latch control stage, the motion equation has different matrix coefficients:

$$\dot{X} = \widetilde{P}X + \widetilde{Q} \tag{16}$$

$$\widetilde{P} = \begin{bmatrix} 0 & 0 & 0 \\ 0 & 0 & 0 \\ 0 & 0 & A' \end{bmatrix}, \widetilde{Q} = 0 \tag{17}$$

For the motion-unlocking stage, in order to improve the power absorption capacity of the WEC array, the damping coefficient is regarded as a function of the significant wave height and peak period. Through real-time monitoring of the wave surface and analysis of wave parameters, the corresponding "optimal motion-limiting damping coefficient" under regular waves is selected by means of differentiation. That is, the motion-limiting system is set as

$$\begin{cases} c_{pL,j}^{(H_s,T_p)}(t) = c_{p,j_opt}^{(H_s(t),T_p(t))}(t), k_{pL,j}(t) = 0 & |z_j(t)| \le L_j \\ c_{pL,j}^{(H_s,T_p)}(t) = c_{p,j_opt}^{(H_s(t),T_p(t))}(t) + c_{L,j}, k_{pL,j}(t) = k_{L,j} & |z_j(t)| > L_j \end{cases} \tag{18}$$

where $H_s(t) = mean(H_s(t - \Delta t, t))$,$T_p(t) = mean(T_p(t - \Delta t, t))$. The wave parameters within the time period Δt before time t are taken as the condition for adjusting the damping. The PTO system damping $c_{p,j}$ at time t is set to the optimal motion-limiting damping coefficient $c_{p,j_opt}^{(H_s(t),T_p(t))}(t)$ under the sea state condition within the preceding Δt time period. At this time, the motion equation of the two-floater array is

$$\dot{X} = \overline{P}X + Q \tag{19}$$

For concise representation, $\overline{P}$ is written in block matrix form:

$$\overline{P} = \begin{bmatrix} 0 & I & 0 \\ P_{21} & \overline{P}_{22} & P_{23} \\ 0 & B' & A' \end{bmatrix} \tag{20}$$

where

$$\overline{P}_{22} = \begin{bmatrix} \frac{-D'_{11} + c_{pL,1}^{(H_s,T_p)}(t)}{M_1 + \mu_{11}(\infty)} & \frac{-D'_{12}}{M_1 + \mu_{11}(\infty)} \\ \frac{-D'_{21}}{M_2 + \mu_{22}(\infty)} & \frac{-D'_{22} + c_{pL,2}^{(H_s,T_p)}(t)}{M_2 + \mu_{22}(\infty)} \end{bmatrix} \tag{21}$$

To verify the effectiveness of the proposed variable parameter control method in improving energy conversion performance, this method is compared with the power absorption capacity of a two-floater array using linear control under a motion-limiting system in irregular waves. Taking the sea state with H_s = 3 m and T = 8 s as an example, the design thresholds of the motion-limiting system are taken as L_1 = 1.2 m and L_2 = 0.8 m, and Δt = 15 s is taken in the variable parameter control method. Under regular waves, the optimal linear damping for Bodies 1 and 2 can be calculated using Equation (3). Under irregular waves, the wave height and period are approximated using the past 15-s wave height time-history, and then the optimal damping is calculated using Equation (3). It should be noted that the 15 s window is not the optimal prediction interval for the rolling wave height and period; rather, it is a subjective choice corresponding to two to three wave periods. Under linear control, $c_{p,1}$ = 197,232 N/(m/s) and $c_{p,2}$ = 297,266 N/(m/s) are taken, which are the optimal damping coefficients corresponding to the two-floater array in the regular wave calculation results. The calculation results are as follows. The end-stop mechanism alters the dynamic behavior of the system to some extent, and the actual optimal PTO damping with end-stops may change, which is closely related to the severity of the sea state (i.e., the wave height) [27]. In this paper, the influence of the end-stop mechanism parameters on the optimal damping coefficient is not considered, and this aspect needs to be addressed in future research.

In a wave energy array, the average power and capture width ratio generated by the j-th wave energy converter are expressed as

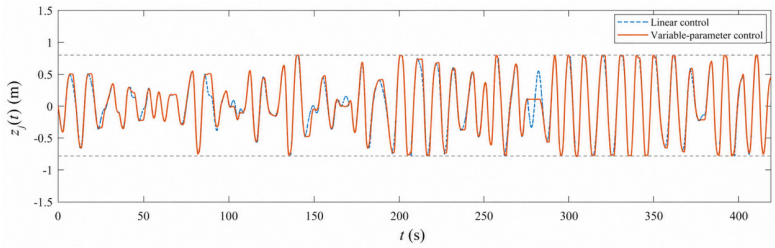
$$\overline{P}_j = \frac{1}{n_p T}\int_{t_s}^{t_s+n_p T} \frac{1}{2} c_{p,j}\dot{z}_j(t)^2 dt \tag{22}$$

$$CWR_j = \frac{\overline{P}_j}{P_{wave} B_j} \tag{23}$$

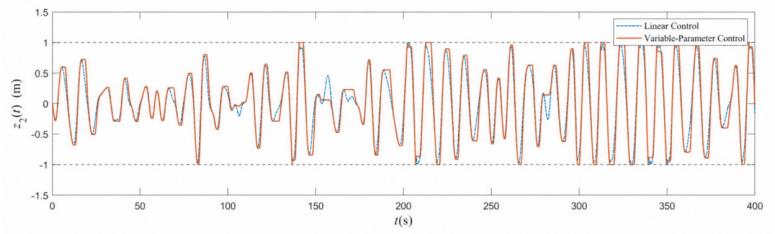
where t_s is the time instant after the motion becomes stable, n_p is the number of wave periods used for calculating the average power, P_{wave} is the wave energy per unit wave crest width, and B_j is the incident wave width of floater j. P_{wave} can be expressed as

$$P_{wave} = \begin{cases} \rho g H_s^2 T_p / 32\pi & \text{, irregular wave} \\ \rho g H^2 T / 64\pi & \text{, regular wave} \end{cases}$$

The displacement time-history curves of the two-floater array under different control methods are shown in Figure 10, where the irregular wave surface profiles generated under the two simulation conditions are strictly identical; therefore, the incident wave excitation forces are the same. Compared with linear control, the fluctuation of the displacement time-history curves of the floating bodies under the variable parameter control method is smoother, exhibiting stronger adaptability to external irregular wave excitation. Meanwhile, the response of the variable parameter control in terms of displacement is more severe, meaning that the proposed method increases the displacement of the floating bodies.



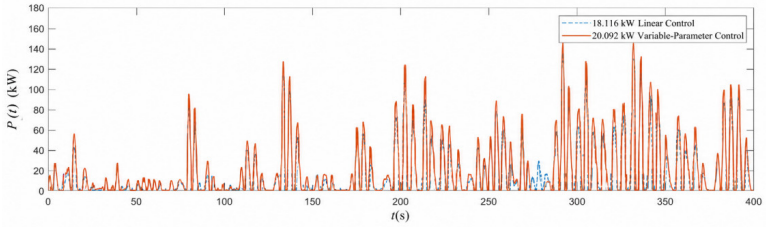
(**a**) Displacement of Floating Body 1 under different control methods



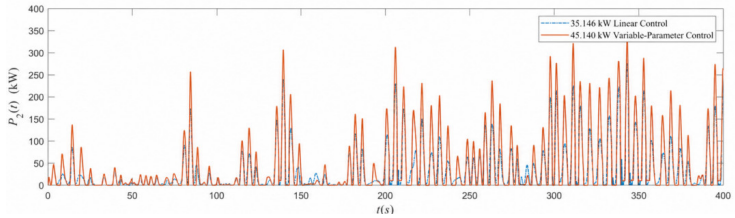
(**b**) Displacement of Floating Body 1 under different control methods

Figure 10. Comparison of displacement time-history curves of the two-floater array.

The increase in the displacement of the floating bodies means that the device can capture more energy from the waves. Figure 11 presents the instantaneous power time-history curves of the two-floater array under the two control methods. It can be seen from the figure that the instantaneous power generated by the device under variable parameter control exhibits larger peaks. With the application of the variable parameter control method, the average power of Floating Body 1 increases from 18.116 kW to 20.092 kW, and the average power of Floating Body 2 jumps from 35.146 kW to 45.140 kW, with increases of 10.9% and 28.4%, respectively. That is, compared with linear control, the use of the variable parameter control method can significantly improve the energy capture capacity of the device.



(**a**) Instantaneous power of Floating Body 1 under different control methods



(**b**) Instantaneous power of Floating Body 2 under different control methods

Figure 11. Instantaneous power time-history curves of the two-floater array under different control methods.

4.3. Analysis of Power Generation Capacity of the Device Under Regular and Irregular Waves

To investigate the influence of wave incidence under different assumptions on the power generation capacity of the WEC array, based on the sea state data distribution in the sea area of 111~113° E, 15.5~17° N, the power generation matrices and energy capture width contour maps are calculated for the following two conditions: first, the two-floater array under the action of the variable parameter control method under irregular wave excitation; second, the two-floater array with the damping coefficient $c_{p,j}$ taken as the optimal motion-limiting damping coefficient c_{p,j_opt} under regular wave excitation.

The power matrices of the two-floater array under different sea states are shown in Figure 12. The power under the optimal motion-limiting damping control under regular wave excitation is significantly higher than that under the variable parameter control under irregular wave excitation. Under regular wave conditions, since the frequency is single, the resonance of the floating bodies can be effectively excited through damping regulation, which is more conducive to improving energy capture. In contrast, under irregular wave conditions, wave excitation is a random process. The corresponding sea state of each grid cell is represented by the average wave height of the largest 1/3 waves and the average peak period within 1 h. Even though phase synchronization is achieved by using latch control and the optimal motion-limiting damping corresponding to the preceding wave conditions within that time period is fed back through real-time wave surface parameters, the time-wise matching between the peak frequency and the damping parameters still cannot be achieved. Under this condition, the power generation of the WEC array is always lower than the former. If short-term wave forecasting is incorporated, the damping can be further matched in the variable parameter control, thereby improving the energy capture under irregular waves.

The annual energy production can be calculated by combining the occurrence hours of sea states with the power matrix of the WEC, and can be expressed as [28]

$$E_0 = \sum_{i=1}^{n} (P_{1,i} + P_{2,i}) \times O_{b,i} \tag{24}$$

where $P_{1,I}$ is the average power generation of WEC 1 under the i-th sea state (in kW), $O_{b,I}$ is the occurrence hours of the i-th sea state (in h), and n is the total number of sea states considered.

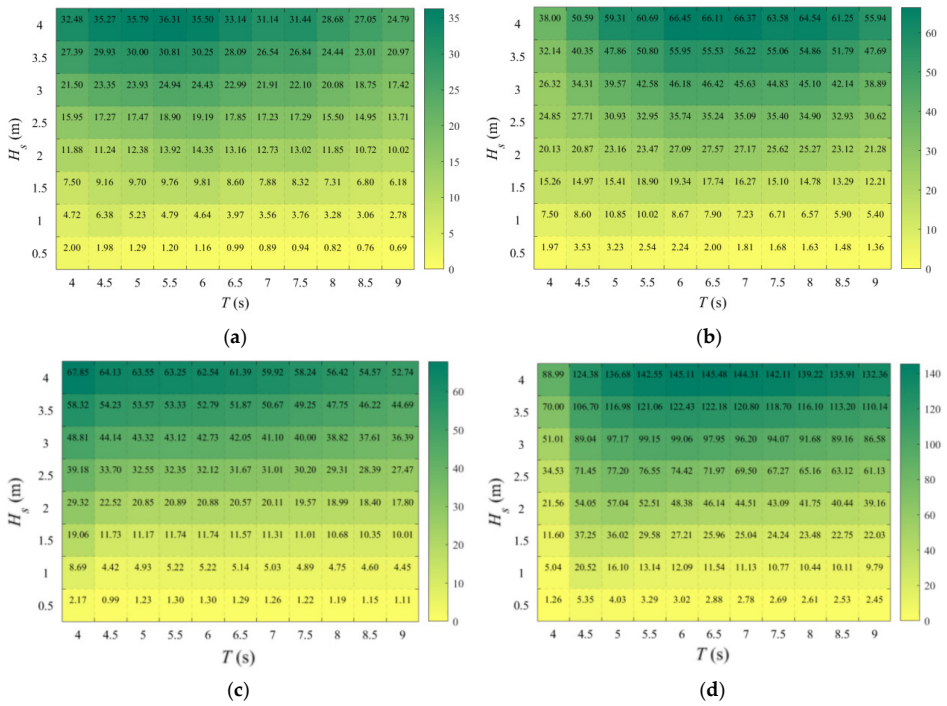


Figure 12. Power matrices of the two-floater array under different sea states (kW). (**a**) Variable parameter control under irregular waves—Floating Body 1 (kW); (**b**) variable parameter control under irregular waves—Floating Body 2 (kW); (**c**) optimal motion-limiting damping control under regular waves—Floating Body 1 (kW); (**d**) optimal motion-limiting damping control under regular waves—Floating Body 2 (kW).

The distribution characteristics of the energy capture width ξ of the two-floater array under different combinations of significant wave height H_s and peak period T are shown in Figure 13. Under the same incidence condition, by comparing the capture widths of the two-floater array, it can be seen that the energy capture width of Floating Body 1 exhibits a peak under short-period sea states and decreases rapidly as the peak period increases, while the peak region of the energy capture width of Floating Body 2 covers a wider range of wave parameters than that of Floating Body 1. In summary, Floating Body 1 has better energy conversion performance in short-period waves, while Floating Body 2 has a higher energy capture width value than Floating Body 1 under the sea states of 111~113° E, 15.5~17° N, and the device exhibits better adaptability to different sea state data. Comparing the incident wave conditions, it can be seen that the capture width peak of the WEC under optimal motion-limiting damping control under regular wave excitation is larger, while the capture width distribution of the WEC under variable parameter control under irregular wave excitation is more uniform, and the overall value is lower than the former.

In the sea area of 111~113° E, 15.5~17° N, the annual total power generation and daily average power generation of the two-floater array WEC are calculated as shown in Table 2. Due to the influence of the physical parameters of the floating bodies themselves, the power generation capacity of Floating Body 2 far exceeds that of Floating Body 1. However, the regular wave condition in the table adopts the optimal motion-limiting damping derived from regular waves, while the irregular wave condition adopts the variable parameter control. The calculation results show that the annual power generation of the former is significantly higher than that of the latter. This difference is the result of the combined effect of wave randomness and control strategy adaptability. On the one hand, under the regular wave assumption, the wave frequency is single, making it easier for the floating bodies to maintain resonance, resulting in higher energy capture efficiency. On the other

hand, in actual irregular waves, the wave parameters are time-varying. Even though variable parameter control is adopted, the phase lag of the control system and the time lag in damping adjustment still lead to partial energy loss. The comparison results in this paper are the sum of the combined effects of wave randomness and control strategy. Therefore, directly using regular waves to replace real sea states for numerical simulation will lead to an optimistic assessment of power generation. Meanwhile, further comparison under the same control strategy is still needed. In the numerical simulation, it is also necessary to base the analysis on the real wave characteristics of the target sea area and incorporate a control strategy that considers time-lag effects, so as to obtain a more accurate and conservative assessment of power generation capacity. In particular, the control strategy in this study considers only power maximization and does not account for factors such as wave surface time-history prediction in real sea states, end-stop loads, control costs, and environmental impacts [29]. The practical applicability and comprehensive performance of the method still require further justification.

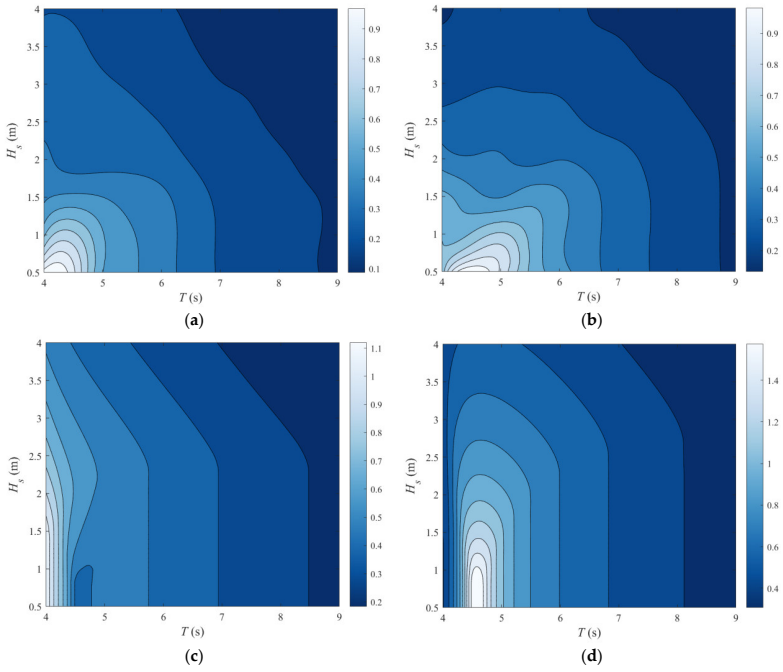


Figure 13. Contour map of the CWR under combinations of significant wave height and peak period (B_1 = 4 m, B_2 = 6 m). (**a**) Variable parameter control under irregular waves—Floating Body 1; (**b**) variable parameter control under irregular waves—Floating Body 2; (**c**) optimal motion-limiting damping control under regular waves—Floating Body 1; (**d**) optimal motion-limiting damping control under regular waves—Floating Body 2.

Table 2. Power generation of the two-floater array WEC.

Power Generation (kWh)	Floating Body 1 (Regular Waves)	Floating Body 1 (Irregular Waves)	Floating Body 2 (Regular Waves)	Floating Body 2 (Irregular Waves)
Annual total power generation	110,768.91	73,536.80	266,490.87	148,881.72
Daily average power generation	313.72	208.27	754.75	421.66

5. Conclusions

This paper takes the sea area of 111~113° E, 15.5~17° N as the research region. Aiming at the problems of poor adaptability of fixed damping control, displacement easily exceeding the design stroke of the PTO system under severe motion conditions, and difficulty in assessing power generation capacity for WEC arrays in real sea states, a systematic study is carried out around three core aspects: motion-limiting system modeling, state-space model replacement of the convolution term, and the variable parameter control method. First, to address the safety hazard of displacement overrun caused by severe heave motion of floating bodies under severe motion conditions, a motion-limiting system model containing a piecewise nonlinear PTO force is established. Through time-domain numerical simulation, the motion time-history curves of the two-floater array with and without the motion-limiting system are compared. The results show that when the motion-limiting thresholds of Floating Body 1 and Floating Body 2 are set to 1.2 m and 0.8 m, respectively, the heave displacement of the floating bodies is strictly limited within the design thresholds, effectively avoiding the risk of displacement overrun under severe motion conditions. Second, to address the problem of low computational efficiency of the convolution term in the time-domain motion equation, a state-space model is adopted to replace the convolution term. The comparison results of the delay function show that the calculation results of the state-space model agree well with the numerical integration method, verifying the feasibility and efficiency of this method in time-domain simulation involving a nonlinear motion-limiting system. On this basis, to address the problem that fixed damping cannot match sea states in real time under irregular waves, combined with the distribution of real sea state data, a variable parameter control method based on latch control is proposed using the optimal motion-limiting damping parameter matrix calculated under regular wave conditions. Taking the sea state with H_s = 3 m and T = 8 s as an example, compared with linear control, the average power of Floating Body 1 under variable parameter control increases from 18.116 kW to 20.092 kW, and that of Floating Body 2 increases from 35.146 kW to 45.140 kW, with increases of 10.9% and 28.4%, respectively, verifying the effectiveness of this method in improving energy capture capacity in random waves. Finally, based on ERA-5 reanalysis data, the annual wave height and period data of the actual sea area in 2022 are statistically analyzed, and the annual power generation of the WEC array under regular wave assumptions and irregular wave conditions is calculated, respectively. The results show that under the regular wave assumption, the annual total power generation of Floating Body 1 and Floating Body 2 is 110,768.91 kWh and 266,490.87 kWh, respectively, while under actual irregular wave conditions, it is only 73,536.80 kWh and 148,881.72 kWh. In addition, the difference in floating body dimensions also has a significant impact on the power generation capacity of the array. Since Floating Body 2 is larger in both size and mass than Floating Body 1, its energy capture width value is generally higher than that of Floating Body 1, and it has stronger adaptability to different sea state data, while Floating Body 1 has better energy conversion performance in short-period waves. The combination of floating bodies of different scales in the array can accommodate the energy capture requirements under different wave conditions. The research results of this paper provide a quantitative basis for the design of motion-limiting systems and the selection of control strategies for WEC arrays in actual sea areas.

Author Contributions: M.J. (Mingze Ji) and S.R. conducted the computations and data analysis comparisons; S.R. handled the data analysis and did the proofreading; M.J. (Mingze Ji) and J.L. did the proofreading and editing; W.L. and X.Z. guided the engineering project and provided the data; M.J. (Meiyu Jiang) drafted the manuscript with others. All authors have read and agreed to the published version of the manuscript.

Funding: This research was funded by the Central Universities Special Project for Forward Design Project (grant No. 3072026ZX2401).

Data Availability Statement: The original contributions presented in this study are included in the article. Further inquiries can be directed to the corresponding author.

Conflicts of Interest: The authors declare no conflicts of interest.

Abbreviations

The following abbreviations are used in this manuscript:

WEC	Wave energy converter
OWC	Oscillating Water Column
BEM	Boundary Element Methods
PTO	Power Take-off
CFD	Computational Fluid Dynamics

References

1. Reguero, B.G.; Losada, I.J.; Méndez, F.J. A global wave power resource and its seasonal, interannual and long-term variability. *Appl. Energy* **2015**, *148*, 366–380. [CrossRef]
2. Valério, D.; Beirão, P.; Costa, D.S.J. Optimisation of wave energy extraction with the Archimedes Wave Swing. *Ocean Eng.* **2007**, *34*, 2330–2344. [CrossRef]
3. Tarrant, K.; Meskell, C. Investigation on parametrically excited motions of point absorbers in regular waves. *Ocean Eng.* **2016**, *111*, 67–81. [CrossRef]
4. Zhao, T.; Li, Z.; Niu, B.; Xie, G.; Shangguan, L.; Zhang, M.; Zhu, Y.; Ma, Y.; Hu, C.; Li, Y. A pendulum-based nanogenerator for high-entropy wave energy harvesting. *Nat. Commun.* **2025**, *16*, 5480. [CrossRef]
5. O'connor, M.; Lewis, T.; Dalton, G. Techno-economic performance of the Pelamis P1 and Wavestar at different ratings and various locations in Europe. *Renew. Energy* **2013**, *50*, 889–900. [CrossRef]
6. Reabroy, R.; Zheng, X.; Zhang, L.; Zang, J.; Yuan, Z.; Liu, M.; Sun, K.; Tiaple, Y. Hydrodynamic response and power efficiency analysis of heaving wave energy converter integrated with breakwater. *Energy Convers. Manag.* **2019**, *195*, 1174–1186. [CrossRef]
7. Zheng, X.; Li, J.; Lai, W.; Rong, S.; Zhou, S. 3DOF numerical simulation and performance analysis of a built-in wave energy converter for marine buoys. *Ocean Eng.* **2026**, *343*, 123358. [CrossRef]
8. Lai, W.; Ji, M.; Li, J.; Yang, H.; Zheng, X. Numerical study and optimal control of an oscillating-body wave energy converter with a hydraulic PTO system. *Energy* **2025**, *339*, 139108. [CrossRef]
9. Das, A.; De, S.; Mandal, B.N. Wave interaction with an elliptic disc submerged in a two-layer fluid. *Appl. Math. Model.* **2023**, *117*, 786–801. [CrossRef]
10. Ancellin, M.; Marchand, P.; Dias, F. Towards high-performance linear potential flow BEM solver with low-rank compressions. *Energies* **2024**, *17*, 372. [CrossRef]
11. Natarajan, S.K.; Cho, I. New Strategy on Power Absorption of a Concentric Two-Body Wave Energy Converter. *Energies* **2023**, *16*, 3791. [CrossRef]
12. Renzi, E.; Abdolali, A.; Bellotti, G.; Dias, F. Wave-power absorption from a finite array of oscillating wave surge converters. *Renew. Energy* **2014**, *63*, 55–68. [CrossRef]
13. Falnes, J.; Kurniawan, A. Fundamental formulae for wave-energy conversion. *R. Soc. Open Sci.* **2015**, *2*, 305–338. [CrossRef]
14. Konispoliatis, D.N.; Mavrakos, S.A. Wave power absorption by arrays of wave energy converters in front of a vertical breakwater: A theoretical study. *Energies* **2020**, *13*, 1985. [CrossRef]
15. Jefferys, E.R. Simulation of wave power devices. *Appl. Ocean Res.* **1984**, *6*, 31–39. [CrossRef]
16. Paul, J. Modelling of General Electromagnetic Material Properties in TLM. Ph.D. Thesis, University of Nottingham, Nottingham, UK, 1998.
17. Armesto, J.A.; Guanche, R.; Jesus, F.; Iturrioz, A.; Losada, I.J. Comparative analysis of the methods to compute the radiation term in Cummins' equation. *J. Ocean Eng. Mar. Energy* **2015**, *1*, 377–393. [CrossRef]
18. Cordonnier, J.; Gorintin, F.; De Cagny, A.; Clément, A.; Babarit, A. SEAREV: Case study of the development of a wave energy converter. *Renew. Energy* **2015**, *80*, 40–52. [CrossRef]
19. Sjökvist, L.; Göteman, M. Peak forces on wave energy linear generators in tsunami and extreme waves. *Energies* **2017**, *10*, 1323. [CrossRef]

20. Wei, Y.; Bechlenberg, A.; van Rooij, M.; Jayawardhana, B.; Vakis, A. Modelling of a wave energy converter array with a nonlinear power take-off system in the frequency domain. *Appl. Ocean Res.* **2019**, *90*, 124–134. [CrossRef]
21. Shahroozi, Z.; Göteman, M.; Engström, J. Experimental investigation of a point-absorber wave energy converter response in different wave-type representations of extreme sea states. *Ocean Eng.* **2022**, *248*, 693–716. [CrossRef]
22. Zheng, X.; Ji, M.; Jing, F.; Lu, Y.; Zheng, W.; Zhou, S.; Li, X.; Yan, H. Sea trial test on offshore integration of an oscillating buoy wave energy device and floating breakwater. *Energy Convers. Manag.* **2022**, *256*, 115375. [CrossRef]
23. Lai, Y.; Hu, G.; He, B.; Ding, J.; Yang, Y. Effects of integration of WECs on the dynamic behavior of a fixed-bottom offshore wind turbine. *Ocean Eng.* **2026**, *363*, 126787. [CrossRef]
24. Zheng, X.; Li, J.; Lai, W.; Rong, S. Vibration characteristics of a oscillating-buoy wave energy converter. *J. Vib. Shock* **2024**, *43*, 1–11. [CrossRef]
25. Aghipour, R.; Perez, T.; Moan, T. Hybrid frequency–time domain models for dynamic response analysis of marine structures. *Ocean Eng.* **2008**, *35*, 685–705. [CrossRef]
26. Babarit, A.; Clément, A.H. Optimal latching control of a wave energy device in regular and irregular waves. *Appl. Ocean Res.* **2006**, *28*, 77–91. [CrossRef]
27. Tan, J.; Zhang, Y.; Jain, A.; Lavidas, G. The Impacts of Power Take-Off Surviving Strategies on the Extreme Load Estimations of Wave Energy Converters. *J. Mar. Sci. Eng.* **2025**, *13*, 994. [CrossRef]
28. Boodoo, A.; Cross, J.; Ridgewell, C.; Kortelainen, V.; Vuorinen, M.; Harouna-Mayer, A. Long-term impacts and design considerations of dual-purpose wave farms for energy generation and coastal protection. *Appl. Energy* **2025**, *401*, 126805. [CrossRef]
29. Boodoo, A. A multi-objective optimization framework for wave farm design: Balancing coastal protection and energy output. *Renew. Energy Focus* **2026**, *58*, 100831. [CrossRef]

Disclaimer/Publisher's Note: The statements, opinions and data contained in all publications are solely those of the individual author(s) and contributor(s) and not of MDPI and/or the editor(s). MDPI and/or the editor(s) disclaim responsibility for any injury to people or property resulting from any ideas, methods, instructions or products referred to in the content.